PHILOSOPHICAL TRANSACTIONS OF THE ROYAL SOCIETY A MATHEMATICAL, PHYSICAL & ENGINEERING SCIENCES

Limit Analysis for Plates: A Simple Loading Problem Involving a Complex Exact Solution

E. N. Fox

Phil. Trans. R. Soc. Lond. A 1972 **272**, 463-492
doi: 10.1098/rsta.1972.0057

LIMIT ANALYSIS FOR PLATES: A SIMPLE LOADING PROBLEM INVOLVING A COMPLEX EXACT SOLUTION

By E. N. FOX
Department of Engineering, University of Cambridge

(*Communicated by Sir John Baker, F.R.S. – Received 8 December 1971*)

CONTENTS

Known exact solutions in limit analysis for rigid perfectly plastic plates are relatively scarce and this has led Wood (1965) to question the soundness of the theory by suggesting that exact solutions may not exist even for apparently simple cases of loading, shape of plate and edge conditions. The alternative explanation for the scarcity is that simple problems may require rather complex exact solutions: this is exemplified in the solution now obtained for a central point load acting on a simply supported rectangular plate, with yielding governed by the square yield criterion. When the aspect ratio (length/breadth) of the

Vol. 272. A. 1228. (Price £0.80; U.S. $2.25) 45 [Published 13 July 1972

rectangle lies in the range 1 to 2.25 approximately, the exact mechanism is relatively complex, involving regions of anticlastic curvature at the corners. From the practical standpoint, the known simple upper bounds of yield-line theory for this problem give the collapse load exactly for aspect ratios greater than about 2.25 and are in error by less than 4 % for smaller aspect ratios.

Notation

Excluding subsidiary symbols appearing only briefly where defined in the text, the notation is given below. The coordinate systems are in the middle plane of the undeformed plate, while moments and shear forces are per unit length along a normal section of the plate.

$2a$	length of rectangular plate
$2b = \sqrt{2}$	breadth of rectangular plate
C	defined by equation (87)
$f(\theta)$	defined by equation (60)
$f_n(z)$	defined by equation (44)
$F(u)$	defined by equation (86) as chosen function in equation (66)
$F_1(u)$	defined by equation (97) as chosen function in equation (88)
$F_2(u)$	parametric function in equation (90)
$G(v)$	defined by equation (97) as chosen function in equation (90)
$h_1,\ h_2$	defined by equation (3)
L	defined in figure 14
$m_0 = 1$	yield moment
$m_1 = m_u$ $m_2 = m_v$	principal moments
$m_r, m_\theta, m_{r\theta}$	component moments in polar coordinates
m_x, m_y, m_{xy}	component moments in rectangular coordinates
$m(u)$	a minimum value of m_v for constant u
$M(u)$	a maximum value of m_v for constant u
$M_e(u)$	value of m_v on edge GK, figure 9
P	collapse load
q_r, q_θ	shear forces in polar coordinates
q_u, q_v	shear forces in orthogonal curvilinear coordinates
r	radial polar coordinate
T	defined by equation (76)
u, v	orthogonal curvilinear coordinates, figure 2
$v_e(u)$	value of v on edge GT, figures 9, 10
$v_1(u)$	value of v for $m_v = M(u)$
$V(y)$	shear reaction along LM, figure 12
w	small deflexion of the plate
x, y	rectangular coordinates
$z = u - v$	
α	angle COE, figures 5, 9, 10
$\gamma = \frac{1}{4}\pi - \alpha$	
ϵ	defined by equation (35)
ζ	defined by equation (85)
θ	angular polar coordinate

θ_1	defined in figure 4
θ_2	defined by equation (52)
κ_1, κ_2	principal curvatures
$\kappa_r, \kappa_\theta, \kappa_{r\theta}$	component curvatures in polar coordinates
$\kappa_u, \kappa_v, \kappa_{uv}$	component curvatures in orthogonal curvilinear coordinates
$\xi = a/b$	
ξ_1	value of ξ at change of mechanism (case 12, table 1)
ξ_2	value of ξ for case 11, table 1
ρ_1, ρ_2	radii of curvature in orthogonal net, figure 2
ρ	radius of curvature of curved edge, figure 3
ϕ	angle relating to orthogonal net, figure 2
$\phi_e(u)$	value of ϕ on edge GT, figure 10
$\chi(u, v)$	defined by equation (26)
$\psi(\alpha)$	defined by equation (31)

1. Introduction

Wood (1965) questioned the soundness of the basic assumptions of limit analysis for rigid perfectly plastic plates loaded in bending, by advancing the tentative hypothesis that exact solutions do not necessarily exist in many problems. He expanded his arguments further at a conference (Wood 1968); primarily, his case rests on the fact that exact solutions, using the square yield criterion of Johansen (1942), have not been found for apparently simple cases of loading, edge conditions and shape of plate. At the same conference, the present author countered Wood's arguments by an existence theorem (Fox 1968) indicating that exact solutions should in general exist for homogeneous isotropic plates under practical types of loading and certain common types of edge condition; and in the discussion he suggested that the scarcity of known exact solutions probably lay in the fact that apparently simple problems may require relatively complex exact solutions. Shortly after this conference, Sawczuk & Hodge (1968) published a paper dealing with the exact solution of problems of simply supported homogeneous isotropic plates under single-point loading, with yield governed by the square criterion; in particular, they gave a solution for a simply supported rectangular plate under a central point load. Unfortunately, this solution is in error for reasons given later,† and it is the purpose of the present paper to give a revised solution showing, in particular, that if the aspect ratio (length/breadth) of the rectangle lies in a certain range the exact solution is relatively complex, involving anticlastic curvature in parts of the deformed surface of the plate.

2. Statement of problem

We consider a rectangular plate of uniform thickness and sides $2a$, $2b$ where $a > b$ simply supported on all edges and subjected to a point load P at its centre. For convenience of nomenclature, we regard the plane of the plate as horizontal, with load and deflexion positive downward and with moments and curvatures taken positive when sagging. The material of the plate is homogeneous and isotropic, and yield in bending is governed by the square

† I am indebted to my colleague, Dr C. T. Morley, for drawing my attention to the error and the need for a revised solution.

yield criterion with a yield moment m_0 per unit length of plate in both sagging and hogging curvatures.

For analysis, we shall effectively work non-dimensionally by choosing m_0 as the unit of force and $b\sqrt{2}$ as the unit of length, this latter being the most convenient choice for simplicity of later algebra. In these units

$$\left.\begin{aligned} m_0 &= 1, \\ b &= 1/\sqrt{2}, \end{aligned}\right\} \tag{1}$$

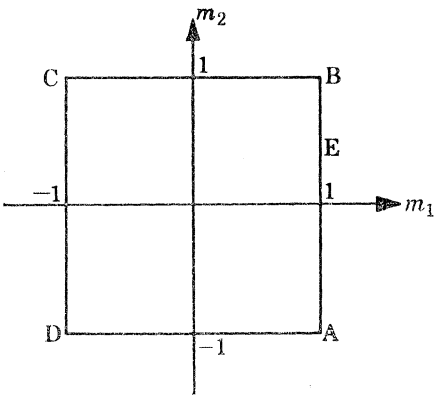

FIGURE 1. Square yield criterion.

and we shall use the term *aspect ratio* and the symbol ξ to denote

$$\xi = a/b = a\sqrt{2} > 1. \tag{2}$$

The conditions for an exact solution of a problem of limit analysis for rigid perfectly plastic plates loaded in bending have been discussed in detail by the author elsewhere (Fox 1968). Here we summarize these conditions for the present problem. First, we define a *statically admissible* moment field as a field which satisfies: (i) equilibrium with the central point load and zero distributed load over the area of the plate, (ii) the condition of zero moment along the simply supported edges, and (iii) the square yield criterion illustrated in figure 1 in terms of principal moments m_1, m_2 per unit length of plate. Thus any deformation occurs only for points on the square ABCD and states corresponding to points outside the square are prohibited. Secondly, we define a *mechanism* as a small virtual deflexion w of the plate such that (*a*) w is continuous and the slopes are at least piecewise continuous over the plate area, and (*b*) $w = 0$ at the edges of the plate.

For an exact solution, we must find a value of the central load P, called the *collapse load*, such that there coexist a statically admissible moment field and a mechanism related at all yielding parts of the plate by the *normality rule* defined below.

The mechanism may contain variously: (i) *rigid leaves* where the plate remains plane and undeformed, though a leaf may deflect as a rigid body, (ii) yielding regions of finite curvature, and (iii) *hinge-lines* corresponding to a discontinuity of slope across a boundary between two regions of the mechanism.

At a point of finite curvature in a yielding region of the mechanism, the *normality rule* can be specified in terms of principal moments (m_1, m_2) and associated principal curvatures (κ_1, κ_2) by the two conditions: (*a*) the directions of the principal curvatures coincide with the principal moment directions, and (*b*) a vector in the (m_1, m_2) plane with components proportional to (κ_1, κ_2)

is in the direction of the outward normal to the yield locus at the associated point (m_1, m_2) on this locus. Thus for the square yield locus of figure 1, the second condition requires that $\kappa_1 > 0$, $\kappa_2 = 0$ for (m_1, m_2) at E on the side AB, while for (m_1, m_2) at the corner A, regarded as the limit of a quadrant of a circle of small radius (Fox 1968), the second condition requires that $\kappa_1 \geqslant 0, \kappa_2 \leqslant 0$, excluding both curvatures zero. On a hinge-line, the normality rule requires that the hinge rotation and yield moment are either both sagging or both hogging so that positive work is done on the plate along the hinge-line.

3. Basic equations

In addition to rectangular coordinates (x, y) and polar coordinates (r, θ) with origin at the centre O in the plane of the undeformed plate, we shall use orthogonal curvilinear coordinates

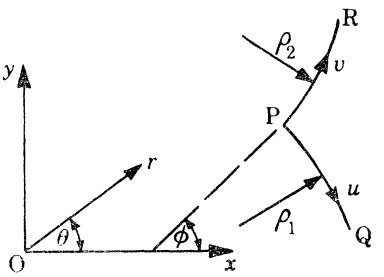

Figure 2. Notation for orthogonal curvilinear coordinates u, v.

(u, v) in this plane, such that at any point, the tangents to the curves u = constant, v = constant through the point are in the principal moment directions. Thus in figure 2, PR is a curve u = constant with principal moment $m_1 = m_u$ and shear force q_u per unit length on a section of the plate tangential to the curve; similarly, for the curve PQ, with v = constant, principal moment $m_2 = m_v$ and shear force q_v. These curves will be termed the *characteristics* of a *moment net* formed by such curves in any region of the plate. We use h_1, h_2, positive by definition, to denote the parameters such that an element of length ds is given by

$$\mathrm{d}s^2 = h_1^2 \mathrm{d}u^2 + h_2^2 \mathrm{d}v^2, \tag{3}$$

while in figure 2, ϕ is the angle between the fixed direction Ox and the tangent at P to the curve PR; and ρ_1, ρ_2 are the radii of curvature of the characteristics, positive as illustrated in figure 2 in relation to the positive directions of u and v. The following known relations for an orthogonal net are easily derived:

$$\left.\begin{aligned} \frac{h_1}{\rho_1} &= \frac{\partial h_1}{h_2 \partial v} = -\frac{\partial \phi}{\partial u}, \\ \frac{h_2}{\rho_2} &= \frac{\partial h_2}{h_1 \partial u} = \frac{\partial \phi}{\partial v}, \end{aligned}\right\} \tag{4}$$

$$\left.\begin{aligned} \frac{\partial x}{h_1 \partial u} &= \sin\phi = \frac{\partial y}{h_2 \partial v}, \\ \frac{\partial x}{h_2 \partial v} &= \cos\phi = -\frac{\partial y}{h_1 \partial u}. \end{aligned}\right\} \tag{5}$$

The principal moments m_u, m_v in a statically admissible field must satisfy the yield inequality

$$-1 \leqslant m_u, m_v \leqslant 1 \tag{6}$$

and also, at points other than the centre of the plate, the equation of equilibrium with zero load. This equation can be written in the form

$$\frac{\partial}{\partial u}\left[\frac{h_2}{h_1}\frac{\partial m_u}{\partial u}+(m_u-m_v)\frac{\partial \phi}{\partial v}\right]+\frac{\partial}{\partial v}\left[\frac{h_1}{h_2}\frac{\partial m_v}{\partial v}+(m_u-m_v)\frac{\partial \phi}{\partial u}\right]=0, \tag{7}$$

while the shear components per unit length of plate are

$$\left.\begin{aligned} q_u &= \frac{m_u-m_v}{\rho_2}+\frac{\partial m_u}{h_1\partial u}, \\ q_v &= \frac{m_v-m_u}{\rho_1}+\frac{\partial m_v}{h_2\partial v}, \end{aligned}\right\} \tag{8}$$

where the positive directions of q_u, q_v are downwards on sections with outward normals in the positive directions of u, v respectively.

The component curvatures associated with the deflected surface $w(u, v)$ of the mechanism are

$$\left.\begin{aligned} \kappa_u &= -\frac{\partial}{h_1\partial u}\left(\frac{\partial w}{h_1\partial u}\right)-\frac{1}{\rho_1}\frac{\partial w}{h_2\partial v}, \\ \kappa_v &= -\frac{\partial}{h_2\partial v}\left(\frac{\partial w}{h_2\partial v}\right)-\frac{1}{\rho_2}\frac{\partial w}{h_1\partial u}, \\ \kappa_{uv} &= -\frac{1}{h_1h_2}\frac{\partial^2 w}{\partial u\partial v}+\frac{1}{\rho_1}\frac{\partial w}{h_1\partial u}+\frac{1}{\rho_2}\frac{\partial w}{h_2\partial v} \end{aligned}\right\} \tag{9}$$

on the small-deflexion theory of plates with sagging curvatures positive.

Since the coordinates (u, v) were defined as specifying the moment characteristics, it follows from the normality rule that these characteristics are also the lines of curvature for the mechanism, with κ_u, κ_v as principal curvatures. The condition $\kappa_{uv} = 0$ then gives a governing differential equation for the deflexion in any yielding region of finite curvature and from (9), with use of (4), this equation can be expressed, as convenient, in either of the forms

$$\frac{\partial}{\partial u}\left(\frac{\partial w}{h_2\partial v}\right)=\frac{1}{\rho_1}\frac{\partial w}{\partial u}, \tag{10}$$

$$\frac{\partial}{\partial v}\left(\frac{\partial w}{h_1\partial u}\right)=\frac{1}{\rho_2}\frac{\partial w}{\partial v}. \tag{11}$$

We note that for regions of the plate where the principal moments are m_r, m_θ in polar coordinates (r, θ), the relevant formulae are given by the substitutions $u = r$, $v = \theta$, $\phi = \frac{1}{2}\pi + \theta$, $h_1 = 1$, $h_2 = \rho_2 = r$, and $1/\rho_1 = 0$ in the preceding formulae.

For use later in applying the second condition of the normality rule, we give now two theorems relating to the junction of different types of surface in the mechanism, when this junction is a line of curvature for both surfaces. In this context, any curve in a plane leaf may be regarded as a line of curvature for this rigid region.

THEOREM I. *If two surfaces of the mechanism join with continuous slopes (no hinge-rotation) on a common line of curvature, then the surfaces have the same principal curvature for a section tangential to the line.*

This theorem follows immediately from the fact that the two surfaces have the same normal at any point of the junction line.

THEOREM II. *The hinge-rotation is constant along a hinge-line which is a line of curvature for the surface of the mechanism on both sides of the hinge-line.*

Consider a line of curvature u = constant and integrate (11) with respect to v along this line between two points where the deflexions are w_1, w_2. Then for either side of the line we obtain

$$\left[\frac{\partial w}{h_1 \partial u}\right]_1^2 = \int_{w_1}^{w_2} \frac{\mathrm{d}w}{\rho_2} \quad (u = \text{constant}), \tag{12}$$

for the change of slope perpendicular to the line. But the right-hand side of (12) involves only w and ρ_2, proper to the line itself, and therefore the left-hand side of (12) is the same for both sides of the line: hence it follows that the hinge rotation is constant along the hinge-line. Similarly, for a line of curvature v = constant, using (10) in place of (11) in the argument.

4. THE MOMENT FIELD

We shall be concerned in particular with yielding regions of the plate corresponding to the corner A of the square yield criterion (figure 1), for which the principal moments and shears are

$$\left.\begin{aligned} m_u &= 1, & m_v &= -1, \\ q_u &= 2/\rho_2, & q_v &= -2/\rho_1, \end{aligned}\right\} \tag{13}$$

whence equation (7) gives

$$\frac{\partial^2 \phi}{\partial u \, \partial v} = 0 \tag{14}$$

as the governing equation for the moment net. This has the general solution

$$\phi = g_1(u) + g_2(v), \tag{15}$$

where g_1 and g_2 are arbitrary functions and the net is of the Hencky–Prandtl type (Prager & Hodge 1951).

At a simply supported edge, the condition of zero edge moment for the field (13) corresponds to the geometrical property that the characteristics of the moment net intersect the edge at an angle of $\frac{1}{4}\pi$. Consider, with reference to figure 3, the general case of a curved simply supported edge of radius of curvature ρ at L. Then $\phi = \frac{1}{4}\pi + \eta$, $h_1 \mathrm{d}u = \mathrm{d}s/\sqrt{2} = h_2 \mathrm{d}v$ along the edge whence, using (4), we obtain

$$\frac{1}{\rho} = \frac{\mathrm{d}\eta}{\mathrm{d}s} = \frac{\mathrm{d}\phi}{\mathrm{d}s} = \frac{\partial \phi}{\partial u}\frac{\mathrm{d}u}{\mathrm{d}s} + \frac{\partial \phi}{\partial v}\frac{\mathrm{d}v}{\mathrm{d}s} = \frac{1}{\sqrt{2}}\left(\frac{1}{\rho_2} - \frac{1}{\rho_1}\right) \tag{16}$$

for the moment net of the field (13) at a simply supported edge.

We now consider the moment-field proposed by Sawczuk & Hodge (1968) for the present problem. This field is specified in terms of the regions of the plate illustrated in figure 4 for the first quadrant, where O is the centre of the plate, CE is a circular arc of centre O, and FD, DT are the halves of two simply-supported edges; there is a similar pattern in each of the other quadrants corresponding to the symmetry of the problem. In the present notation, the Sawczuk–Hodge field is as follows, using polar coordinates with origin O for the regions meeting at O:

triangle OFC

$$\left.\begin{aligned} m_\theta &= 1, & m_r &= -\cot^2\theta, & m_{r\theta} &= 0 \\ q_\theta &= 0, & q_r &= -(\operatorname{cosec}^2\theta)/r \end{aligned}\right\} \ \tfrac{1}{4}\pi \leqslant \theta \leqslant \tfrac{1}{2}\pi; \tag{17}$$

sector OCE

$$\left.\begin{aligned} m_\theta &= 1, \quad m_r = -1, \quad m_{r\theta} = 0 \\ q_\theta &= 0, \quad q_r = -2/r \end{aligned}\right\} \theta_1 \leqslant \theta \leqslant \tfrac{1}{4}\pi; \tag{18}$$

triangle ODT

$$\left.\begin{aligned} m_\theta &= 1, \quad m_r = -\tan^2\theta, \quad m_{r\theta} = 0 \\ q_\theta &= 0, \quad q_r = -(\sec^2\theta)/r \end{aligned}\right\} 0 \leqslant \theta \leqslant \theta_1 < \tfrac{1}{4}\pi. \tag{19}$$

All the above fields have simple radial and circular characteristics and are statically admissible.

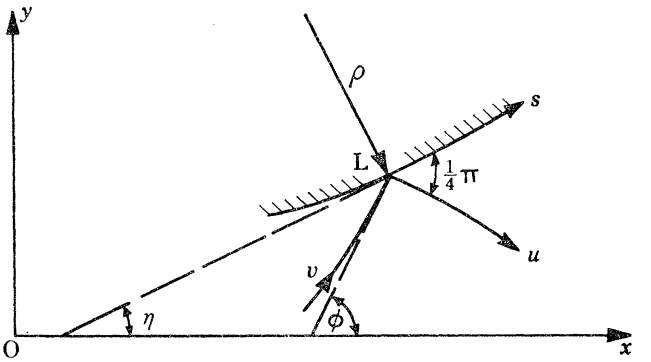

FIGURE 3. Moment net at simply supported edge.

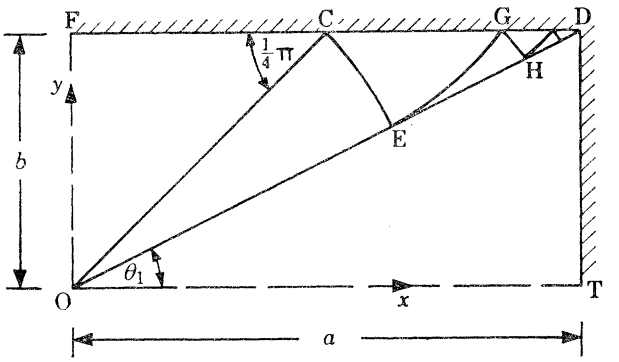

FIGURE 4. Regional pattern of Sawczuk–Hodge solution.

Region CED

The field is given by (13) with the characteristics forming a Hencky–Prandtl net in which CE is a given characteristic v = constant and all characteristics intersect the edge CD at $\frac{1}{4}\pi$.

The associated central collapse load was evaluated by Sawczuk & Hodge and for $\xi > 1$ it is less than the upper bound value

$$P = 4\left(\frac{a}{b} + \frac{b}{a}\right) \tag{20}$$

given by yield-line theory using the mechanism of a symmetrical pyramid on the rectangle as base. But in contradiction, since from (19) the moment along the diagonals is everywhere at the yield value $m_\theta = 1$ in the Sawczuk–Hodge field, the use of virtual work with the pyramid mechanism shows that if this field were in equilibrium with no load other than a central point load, then this load is given by (20) and not the lower value proposed by Sawczuk & Hodge.

The cause of the contradiction lies in the field postulated for the region CED which involves two types of Hencky–Prandtl net. Thus in CEG, the net is regular with the boundary EG as a characteristic u = constant, whence from (13) there is a shear force $q_u = 2/\rho_2$ per unit length on

EG, *acting downwards on* CEG. But in the adjoining region EGH, the boundary EG is not itself a characteristic but is an envelope of straight characteristics u = constant, and it can be shown that this requires a shear force $2/\rho_2$ per unit length on EG, *acting downwards on* EGH. Hence such a junction of nets involves a discontinuity of shear force which violates equilibrium in the absence of an applied line load of intensity $4/\rho_2$ along the junction. The same type of discontinuity invalidates other proposals of Sawczuk & Hodge (1968) for point loads on simply supported plates.

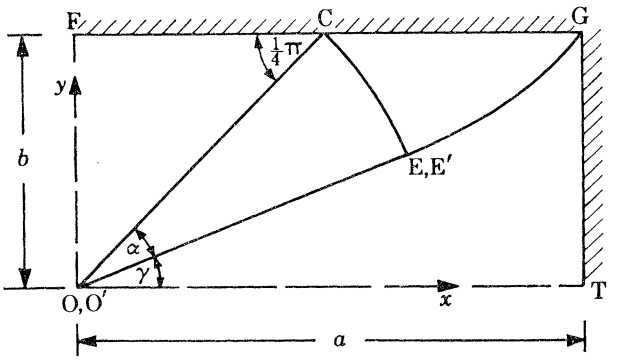

FIGURE 5. Regional pattern of present solution for $1 \leqslant \xi = a/b \leqslant \xi_1$. (O′, E′ are points in mechanism corresponding to O, E in undeformed plate.)

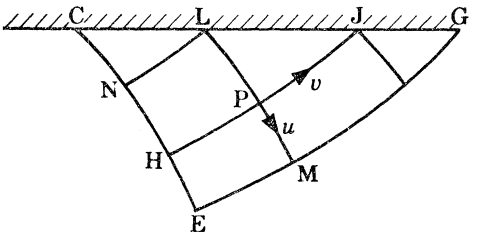

FIGURE 6. Hencky–Prandtl net in region CEG of figure 5.

As the first step in seeking the correct solution, we modify the Sawczuk–Hodge field of figure 4 by omitting the region EGD and expanding the regions OCE and CEG to subdivide the plate quadrant in the four regions shown in figure 5. A statically admissible field is then formed as follows by fields in the various regions.

Regions OFC, OCE (figure 5)

The fields (17) and (18) with the range of (18) extended to $\frac{1}{4}\pi - \alpha \leqslant \theta \leqslant \frac{1}{4}\pi$, together give a statically admissible field in the combined region OFCE.

Region CEG (figure 5)

The field (13) is assumed in this region, and we then need to show that a Hencky–Prandtl net exists such that (*a*) the circular arc CE is a characteristic v = constant, which will ensure equilibrium at this junction with the field (18) in OCE; and (*b*) the characteristics intersect the edge CG at $\frac{1}{4}\pi$ to satisfy the simply supported condition of zero edge moment.

We take $v = 0$ on the characteristic CE with origin $u = 0$, $v = 0$ at C and we then define u, v as follows with reference to figure 6. First, the value u = constant on the characteristic HPJ is defined as equal to the clockwise angular rotation of the tangent to CE between C and the end H of the characteristic. Secondly, the value v = constant on the characteristic LPM is defined as

equal to the value of u on the associated characteristic LN (u = constant) through the common edge point L. With this choice, $\phi = \frac{1}{4}\pi - u$ when $v = 0$ and $\phi = \frac{1}{4}\pi$ when $u = v$, whence the general form (15) becomes

$$\phi = \tfrac{1}{4}\pi - u + v. \tag{21}$$

We substitute (21) in the basic relations (4) to obtain

$$\left.\begin{aligned} \rho_1 = h_1 = \partial h_2/\partial u = \partial \rho_2/\partial u, \\ \rho_2 = h_2 = \partial h_1/\partial v = \partial \rho_1/\partial v, \end{aligned}\right\} \tag{22}$$

whence, in terms of ρ_1, we obtain the differential equation

$$\partial^2 \rho_1/\partial u \partial v = \rho_1. \tag{23}$$

Now from equation (1) the circular arc CE is of unit radius, whence one boundary condition for the net is

$$\rho_1 = 1, \quad v = 0. \tag{24}$$

The other boundary condition for the net is (16) with $1/\rho = 0$, $u = v$ on the straight edge CG, whence using (22), we have

$$\rho_1 = \partial \rho_1/\partial v, \quad u = v. \tag{25}$$

The solution of (23) subject to the boundary conditions (24) and (25) is easily obtained by assuming an expansion of ρ_1 as a power series in u with coefficients as functions of v to be determined from (23) to (25). We find, using (22),

$$\left.\begin{aligned} h_1 = \rho_1 = \chi(u, v); \quad h_2 = \rho_2 = \chi(v, u), \\ \chi(u, v) = 1 + v + \sum_{n=1}^{\infty} \frac{u^n}{n!}\left[\frac{v^n}{n!} + \frac{v^{n+1}}{(n+1)!}\right]. \end{aligned}\right\} \tag{26}$$

The function χ can be expressed in closed form in terms of Bessel functions, but without apparent advantage, since the series in χ is very rapidly convergent for computation over the relevant ranges $0 \leqslant v \leqslant u \leqslant \alpha \leqslant \frac{1}{4}\pi$ for the region CEG. We note that $\rho_1 > 0$, $\rho_2 > 0$ so that the curvatures of the characteristics are of the signs illustrated in figure 6 over the whole region CEG.

For computation, the angle α (figure 5) is taken as the basic parameter with the aspect ratio ξ subsequently found as a function of α. Thus on the edge CG, $u = v$ and the length element is $\sqrt{(2)}\, h_1 \mathrm{d}u$ so that the length CG is given by

$$a - b = \sqrt{2} \int_0^{\alpha} h_1 \mathrm{d}u, \quad v = u, \tag{27}$$

whence using (26), (1) and (2) we find

$$\xi = \frac{a}{b} = 1 + 2\alpha + \sum_{n=1}^{\infty} \left(\frac{\alpha^n}{n!}\right)^2 \left(1 + \frac{2\alpha}{2n+1}\right), \tag{28}$$

in which the series is rapidly convergent for $0 \leqslant \alpha \leqslant \frac{1}{4}\pi$.

Finally, to plot the characteristics, the coordinates (x, y) of nodes in the net could be found from (5) by integrating with respect to v for u constant, using (21), (26) and the known coordinates on the arc CE where $v = 0$, $\phi = \theta = \frac{1}{4}\pi - u$.

Region OEGT (figure 5)

As the boundary of this region is not a simple shape, the determination of a statically admissible field is not straightforward and it was found necessary to use direct numerical evaluation for part

of the field, as described later. Here we note that for any such field, the contribution P_1 (say) to the central load P can be obtained before finding the field, by taking moments about the edge GT for equilibrium of the leaf OEGT as a whole. There is zero moment on the edge and zero shear and twisting moment on the symmetry boundary OT. Hence, the equation for overall equilibrium of OEGT, taking moments about the edge GT, involves only P_1 at O and the moments and shears on the boundary OEG, which are known by continuity from the fields previously found for OEC and CEG. From (18) and (13), there is unit moment along OEG and zero shear on OE, while on EG the shear q_u is given by (13). Now EG is the characteristic $u = \alpha$ of the moment net found for CEG, whence an element of shear force is $q_u h_2 \mathrm{d}v = 2\,\mathrm{d}v$ from (13) and (22), and the overall equilibrium equation is

$$P_1 a = b + 2\int_0^\alpha (a - x)\,\mathrm{d}v = b + 2\int_0^\alpha v\left(\frac{\partial x}{\partial v}\right)\mathrm{d}v, \tag{29}$$

after integration by parts along EG. Then using (1), (2), (5), (21), (26) with $u = \alpha$ we obtain

$$P_1 = [1 + 2\psi(\alpha)]/\xi, \tag{30}$$

where

$$\left.\begin{aligned} \psi(\alpha) &= (1+\alpha)\,T_1 + \sum_{n=1}^{\infty} \frac{\alpha^n}{n!}(\alpha + n + 1)\,T_{n+1}, \\ T_n &= \sqrt{2}\int_0^\alpha \frac{v^n}{n!}\cos\left(\tfrac{1}{4}\pi - \alpha + v\right)\mathrm{d}v, \end{aligned}\right\} \tag{31}$$

and ξ is given by (28).

The values of T_n can be computed from elementary integrals for T_1, T_2 and a reduction formula for larger n; the resulting series for $\psi(\alpha)$ is rapidly convergent for the relevant range $0 \leqslant \alpha \leqslant \frac{1}{4}\pi$.

5. The collapse load

For the plate quadrant (figure 5), the three regions OFC, OCE and OEGT contribute 1, 2α and P_1 respectively to P whence the collapse load for the whole plate is given by

$$P = 4 + 8\alpha + 4P_1, \tag{32}$$

where P_1 is given by (30).

From (32) and (28), the values of P and ξ have been computed at intervals of $\frac{1}{400}\pi$ in α to give the curve QRS in figure 7. Also in this figure, the curve QLM and the line LRT are known upper bounds of yield-line theory, with QLM given by (20) for the pyramid mechanism, while LRT is the upper bound

$$P = 4 + 2\pi \quad (\xi \geqslant \sqrt{2}), \tag{33}$$

obtained from the symmetrical mechanism illustrated in plan by figure 8. Here, O is the centre of the plate $G_1G_2G_3G_4$, while C_1OC_3, C_2OC_4 intersect the edges at $\frac{1}{4}\pi$ and $C_4W_1C_1$, $C_2W_2C_3$ are arcs of a circle, centre O. In the mechanism, the portions C_1OC_2, C_3OC_4 deflect as rigid leaves to become opposite faces of a pyramid, vertex below O, while $OC_1W_1C_4$, $OC_2W_2C_3$ deflect and deform to become the opposite quarters of a circular cone with the same vertex as the pyramid. The plate outside this central region remains rigid and undeformed in its original plane.

In figure 7, the curve QRS intersects the line LRT at R corresponding by computation to rounded values

$$\left.\begin{aligned} \xi_1 &= 2.2456 \\ \alpha &= 0.47019 \end{aligned}\right\} \quad (P = 4 + 2\pi), \tag{34}$$

defining ξ_1 (for later brevity) as the abscissa of R.

PHILOSOPHICAL TRANSACTIONS OF THE ROYAL SOCIETY A MATHEMATICAL, PHYSICAL & ENGINEERING SCIENCES

It is clear that the field of figure 5 leading to the curve QRS cannot give the exact solution for $\xi > \xi_1$. Instead we assert that for $1 \leqslant \xi \leqslant \xi_1$ the exact collapse load is given by the portion QR of the curve QRS, derived from (28) and (32), while for $\xi \geqslant \xi_1$ it is given by the line RT, corresponding to (33), with a change of mechanism when $\xi = \xi_1$ at R. This assertion will be justified as follows:

$1 \leqslant \xi \leqslant \xi_1$. The moment field is that illustrated in figure 5, for which we have already defined statically admissible fields in the regions OCF, OCE and CEG, while later we show that a statically admissible field can be found in the remaining region OEGT for this range of ξ. The associated mechanism is derived and justified in the next section of the paper.

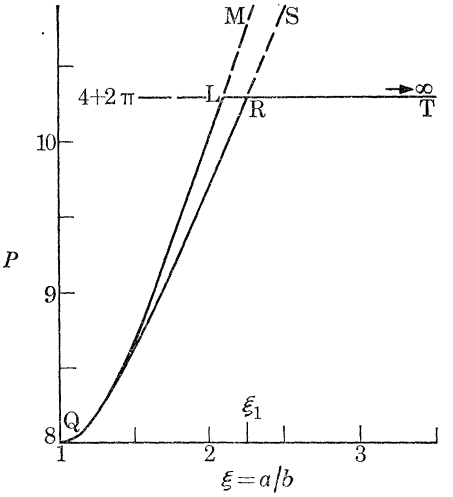

FIGURE 7. Collapse load for central point load on a simply supported rectangular plate. QL–LT, yield-line theory; QR–RT, present solution.

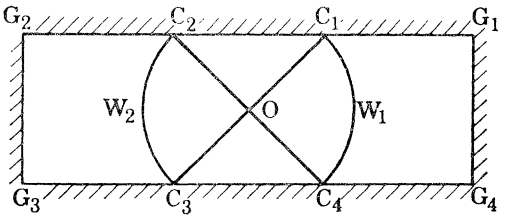

FIGURE 8. Regional pattern for $\xi \geqslant \xi_1$.

$\xi \geqslant \xi_1$. The mechanism is the pyramid cum circular cone already described (figure 8). Then moment fields of the type given by (17) and (18) for the first quadrant (with $\theta_1 = 0$) are statically admissible for the central region $C_1C_2W_2C_3C_4W_1C_1$ (figure 8); and it is easily verified that these fields satisfy the normality rule in relation to the mechanism. It remains only to show later that there is a statically admissible field in the outer portions of the rectangle where the plate is undeformed and the normality rule is irrelevant.

The above behaviour of the exact solution, with the field of figure 5 invalid for $\xi > \xi_1$ indicates that when seeking exact solutions it is wise to evaluate the collapse load at the earliest possible stage of the analysis, since if it exceeds a known upper bound, time will not be wasted in seeking statically admissible fields which do not exist.

It will be seen from figure 7 that the upper bounds QL-LT of yield-line theory give close estimates of the exact collapse load QR–RT, with a maximum error of 3.6 % occurring at L.

A better upper bound than QL can be obtained as a particular case of more general results given by Mansfield (1957) who used the calculus of variations to derive the best upper bounds for wider classes of mechanisms than those of simple yield-line theory. In the present problem, a mechanism corresponding to Mansfield's figure 17 and his equations (29) to (32) gives an upper bound curve lying between QL and QR in figure 7, with a maximum error of 2.9 % where it intersects LT. Thus in this particular case, where simple yield-line theory gives a close estimate of the exact collapse load, the gain in using Mansfield's upper bound is only marginal and the curve for this bound is not shown in figure 7 as it lies too close to QL for clarity.

6. The mechanism for $1 \leqslant \xi \leqslant \xi_1$

6.1. *General description*

With reference to figure 5, the mechanism is specified as follows for the first quadrant. The region OEGT remains plane and undergoes a small rotation ϵ about the edge GT so that the points O and E move to deflected positions O′ and E′ respectively and the deflexion w in this region is given by

$$w = \epsilon(a-x) \quad (\epsilon > 0). \tag{35}$$

Secondly, for the region CEG we shall later derive an anticlastic surface CE′G, passing through the edge CG and intersecting the plane (35) in GE′. This surface then defines deflexions of the mechanism along CE′, and for the sector OCE the mechanism is the general conical surface with generators joining the vertex O′ to points on CE′. Lastly, O′FC is a plane rigid leaf containing the edge FC of the plate and the generator O′C of the cone. Using symmetry and the same vertex O′, we see that the mechanism is similar in the other three quadrants of the rectangle, with no discontinuities of deflexion or slope where plane rigid leaves join on the axes Ox, Oy.

To justify the foregoing as an exact mechanism we need (*a*) to derive an anticlastic surface CE′G satisfying the normality rule in relation to the associated moment field derived in §4; (*b*) to show that the normality rule is satisfied by the conical surface O′CE′ and the field (18); and (*c*) to verify that the normality rule is satisfied on any hinge-lines at the junctions O′C, CE′, O′E′G.

6.2. *The anticlastic surface* CE′G

We use the coordinates (u, v) defining the moment net as in §4 and then by the normality rule $\kappa_{uv} = 0$, whence from (9),

$$\frac{1}{h_1 h_2}\frac{\partial^2 w}{\partial u \partial v} - \frac{1}{\rho_1 h_1}\frac{\partial w}{\partial u} - \frac{1}{\rho_2 h_2}\frac{\partial w}{\partial v} = 0 \tag{36}$$

is the governing equation for the deflexion $w(u, v)$.

The associated boundary conditions are first, the condition on the edge CG (figure 5) that

$$w = 0, \quad u = v, \tag{37}$$

and secondly, equation (35) for $u = \alpha$ on E′G. But since (37) covers (35) for the common point G, we can replace (35) by the condition that the slope $\partial w/h_2 \partial v$ of the anticlastic surface along GE′ is the same as that of the plane (35), whence using (5) and (21), we find

$$\partial w/h_2 \partial v = -\epsilon \cos(\tfrac{1}{4}\pi - \alpha + v), \quad u = \alpha. \tag{38}$$

To solve (36), subject to (37) and (38), we derive associated equations involving only the slope $\partial w/h_2 \partial v$. Thus, as noted earlier, the condition (36) giving $\kappa_{uv} = 0$, can be expressed in either of the

forms (10) and (11), and since $\rho_1 = h_1$, $\rho_2 = h_2$ by (22) for the present net, these forms of (36) can be written

$$\left.\begin{aligned}\frac{\partial}{\partial u}\left(\frac{\partial w}{h_2\,\partial v}\right) &= \frac{\partial w}{h_1\partial u},\\ \frac{\partial}{\partial v}\left(\frac{\partial w}{h_1\partial u}\right) &= \frac{\partial w}{h_2\partial v},\end{aligned}\right\} \tag{39}$$

whence, eliminating $\partial w/h_1\partial u$, we obtain

$$\frac{\partial^2}{\partial u\partial v}\left(\frac{\partial w}{h_2\partial v}\right) = \frac{\partial w}{h_2\partial v} \quad (0 \leqslant v \leqslant u \leqslant \alpha). \tag{40}$$

Also, equation (37) implies zero component slope along the edge CG which intersects the characteristics at $\frac{1}{4}\pi$, whence with use of (39)

$$\frac{\partial w}{h_2\partial v} = -\frac{\partial w}{h_1\partial u} = -\frac{\partial}{\partial u}\left(\frac{\partial w}{h_2\partial v}\right), \quad u = v. \tag{41}$$

Thus the slope $\partial w/h_2\partial v$ must satisfy the differential equation (40) and the boundary conditions (38) and (41), and if we assume the form

$$\frac{\partial w}{h_2\partial v} = -\epsilon\cos\left(\tfrac{1}{4}\pi - u + v\right) - \epsilon\sqrt{2}\sum_{n=1}^{\infty}\frac{(\alpha-u)^n}{n!}f_n(u-v), \tag{42}$$

then (38), (40) and (41) are satisfied if

$$\left.\begin{aligned}f_1'(z) &= 0\\ f_1(0) &= 1\end{aligned}\right\}, \quad \left.\begin{aligned}f_{n+1}'(z) &= f_n(z) + f_n''(z)\\ f_{n+1}(0) &= f_n(0) + f_n'(0)\end{aligned}\right\} n \geqslant 1, \tag{43}$$

where $z = u - v$.

The solution of the recurrence relations (43) can be verified to be the following polynomials involving binomial coefficients:

$$\left.\begin{aligned}f_1(z) &= 1,\\ f_{2j}(z) &= \sum_{i=1}^{j} {}^{2j-1}C_{j+i-1}\left(\frac{z^{2i-1}}{(2i-1)!} + \frac{z^{2i-2}}{(2i-2)!}\right),\\ f_{2j+1}(z) &= {}^{2j}C_j + \sum_{i=1}^{j} {}^{2j}C_{j+i}\left(\frac{z^{2i}}{(2i)!} + \frac{z^{2i-1}}{(2i-1)!}\right),\end{aligned}\right\} \tag{44}$$

for $j \geqslant 1$, and with the usual convention $0! = 1$ in relevant terms.

With the use of (44), the series (42) is rapidly convergent for the relevant ranges

$$0 \leqslant v \leqslant u \leqslant \alpha \leqslant \tfrac{1}{4}\pi,$$

whence $\partial w/h_2\partial v$ could be easily computed if desired. Then using (37), we could compute the deflexion at any point (u, v) by

$$w = -\int_v^u \left(\frac{\partial w}{h_2\partial v}\right) h_2\,\mathrm{d}v, \quad u = \text{constant}, \tag{45}$$

where h_2 is given by (26).

From (39) and (42), the other component slope is

$$\frac{\partial w}{h_1\partial u} = -\epsilon\sin\left(\tfrac{1}{4}\pi - z\right) + \epsilon\sqrt{2}\left[1 + \sum_{n=1}^{\infty}\frac{(\alpha-u)^n}{n!}\left(f_{n+1}(z) - f_n'(z)\right)\right], \tag{46}$$

where $z = u - v$. We can then substantiate (42) and (46) in (9) to obtain expressions for the principal curvatures κ_u and κ_v. These simplify with use of (22) and (43) to give

$$\left.\begin{aligned} \frac{h_1\kappa_u}{\epsilon\sqrt{2}} &= 1 + z + \sum_{n=1}^{\infty} \frac{(\alpha-u)^n}{n!}\left[\int_0^z f_{n+1}(z)\,\mathrm{d}z + f_{n+1}(0)\right], \\ \frac{h_2\kappa_v}{\epsilon\sqrt{2}} &= -1 - \sum_{n=1}^{\infty} \frac{(\alpha-u)^n}{n!} f_{n+1}(z). \end{aligned}\right\} \tag{47}$$

Now $z = u - v \geqslant 0$, $\alpha - u \geqslant 0$ in CEG (figure 5), whence from (44) all $f_n \geqslant 0$ and it then follows from (47) that $\kappa_u > 0$, $\kappa_v < 0$ throughout the region which satisfies the normality rule in relation to the associated field (13) corresponding to the corner A of the square yield criterion (figure 1). We have thus derived an anticlastic surface satisfying the given boundary conditions on CG and GE′ and both conditions of the normality rule as defined earlier in terms of principal moments and curvatures.

Next, we need to examine the possible hinge rotation at the junction GE′ of the anticlastic surface and the plane (35). At this junction, with the sign conventions of figure 6, the sagging hinge rotation is

$$\left(\frac{\partial w}{h_1 \partial u}\right)_{\mathrm{a}} - \left(\frac{\partial w}{h_1 \partial u}\right)_{\mathrm{p}} \quad (u = \alpha), \tag{48}$$

where the suffices refer to anticlastic and plane surfaces respectively. Now from (35), (5) and (21), the component slope $\partial w/h_1\partial u$ for the plane is equal to the trigonometrical first term in the expression (46) for the corresponding component slope in the anticlastic surface. Hence using $u = \alpha$, we find from (48) and (46) a sagging hinge rotation $\epsilon\sqrt{2} > 0$, which satisfies the normality rule in relation to the sagging moment $m_u = 1$ along GE.

6.3. *The conical surface* O′CE′

In polar coordinates r, θ with origin at O (figure 5) in the undeformed plate, the curvature components on small deflexion theory are

$$\kappa_r = -\frac{\partial^2 w}{\partial r^2}, \quad \kappa_\theta = -\frac{\partial^2 w}{r^2 \partial\theta^2} - \frac{1}{r}\frac{\partial w}{\partial r}, \quad \kappa_{r\theta} = -\frac{\partial}{\partial r}\left(\frac{1}{r}\frac{\partial w}{\partial \theta}\right), \tag{49}$$

and since the deflexion on the conical surface varies linearly with r it follows that $\kappa_{r\theta} = 0$, $\kappa_r = 0$ and that κ_θ is of the form $\Phi(\theta)/r$. Thus the lines of curvature are radii and circles in plan and coincide with the characteristics of the field (18) in agreement with the normality rule. This rule also requires first $\kappa_r \leqslant 0$ which is satisfied since $\kappa_r = 0$, and secondly $\kappa_\theta \geqslant 0$ which will be verified later.

At E′ (figure 5), the slopes normal to CE′ in the conical surface and in the anticlastic surface are equal to the slopes along O′E′G on either side of E′. But O′E′G lies in the plane leaf O′E′GT with O′E′ tangential to E′G at E′ so the slope along O′E′G is continuous at E′. Hence there is no hinge rotation about CE′ at E′, and by theorem II (§3) there is no hinge rotation anywhere along CE′, so that the conical surface and the anticlastic surface join with continuous slopes along CE′. Then by theorem I, the curvature component κ_θ on CE′ in the conical surface is equal to $\kappa_u > 0$ in the anticlastic surface. Hence, since κ_θ is of the form $\Phi(\theta)/r$, it follows that $\kappa_\theta > 0$ everywhere on the conical surface in accordance with the normality rule for the field (18).

Again at E′, the slopes normal to O′E′G in the conical surface and in the anticlastic surface are both equal to the slope at E′ along the junction CE′, while the other side of O′E′G is a continuous plane surface. Hence the constant sagging hinge rotation shown earlier to hold on GE′, is

continuous across CE′ at E′ to give a sagging rotation $\epsilon\sqrt{2}$, constant by theorem II along O′E′, conforming with the normality rule in relation to the sagging moment $m_\theta = 1$ on OE.

Lastly, since slopes are continuous both in the conical surface and the anticlastic surface, and also across the junction CE′, it follows that the mechanism has continuous slopes everywhere in the combined surface O′CGE′O′. Then at C, this surface and the plane O′CF have the same slope along the junction O′C and the same zero slope along the edge FCG, whence the slope normal to the junction is also the same and there is no hinge rotation along O′C at C. Then by theorem II, there is zero hinge rotation everywhere along O′C and no check on the normality rule for a hinge line is necessary.

Summing up, the mechanism in the first quadrant (figure 5) consists of four regions: (*a*) a plane rigid leaf O′FC, (*b*) a conical surface O′CE′, (*c*) an anticlastic region CE′G, and (*d*) a plane rigid leaf O′E′GT. The first three regions form a combined surface of continuous slope but there is a sagging hinge-rotation of $\epsilon\sqrt{2}$ along the junction of this combined surface and the plane O′E′GT. It will be noted that for a square plate ($\xi = 1$), the conical and anticlastic surfaces vanish to leave a pyramid mechanism with a sagging hinge-rotation of $\epsilon\sqrt{2}$ on the edges of the pyramid corresponding to the diagonals of the square in plan.

7. Determination of a statically admissible moment field in the rigid region OEGT (figure 5) when $1 \leqslant \xi \leqslant \xi_1$

7.1. *General procedure*

For this region, which is not of simple shape, it was found necessary to obtain a statically admissible field by numerical computation for part of the region. The general procedure for seeking a numerical solution was as follows: with the use of coordinates u, v (figure 2), corresponding to a moment net with principal moments m_u, m_v, a particular form of net and a particular expression for m_u were chosen in order to leave a determinate problem for finding m_v from the equilibrium equation (7) and relevant boundary conditions. Then to satisfy the yield conditions, the forms chosen for the net and m_u were varied where necessary. This method enabled a relatively fine mesh to be used without excessive computing demands. The success of the method depends on the fact that in a rigid region of an exact mechanism, there will in general be an infinite number of statically admissible fields and the choice of the net and a form for m_v will not be critical except possibly near a boundary where the boundary condition requires m_u and/or m_v to be at the yield value. In the present problem, analytical investigations of the form of solution near the yielding boundary EG (figure 5) were used where necessary to indicate suitable choices of net and m_u.

All calculations were carried out on the Cambridge University computer Titan with the normal precision of about 11 decimal digits for this machine. The calculations were performed for the 12 cases of table 1 where the cases 1 to 11 correspond to intervals $\frac{1}{80}\pi$ in α, while case 12 is $\xi = \xi_1$.

7.2. $1 < \xi \leqslant \sqrt{2}$

For this range of ξ, the continuation of the circular arc CE (figure 5) into the region OEGT intersects the edge GT, and the moment field in OEGT can be considered in terms of the three regions illustrated in figure 9.

In the sector OEK, we use the simple radial field

$$\left.\begin{aligned} m_\theta &= 1, \quad m_r = f(\theta), \quad m_{r\theta} = 0, \\ q_\theta &= 0, \quad q_r = (f(\theta) - 1)/r, \end{aligned}\right\} \tag{50}$$

where $f(\theta)$ will be specified later. The field is in equilibrium with zero load except for a point load at O, and it satisfies continuity of normal moment and shear with the adjoining field (18) in OCE, across the common characteristic OE. The field (50) is statically admissible if $|f(\theta)| \leqslant 1$.

In the region OKT, we use the radial field (19) with range now θ_2 for θ_1. This field is statically admissible since it satisfies (i) equilibrium with zero load apart from a point load at O, (ii) continuity of normal moment and shear with the field (50) across the common characteristic OK, (iii) zero shear and twisting moment on the symmetry line OT, and (iv) the yield inequality.

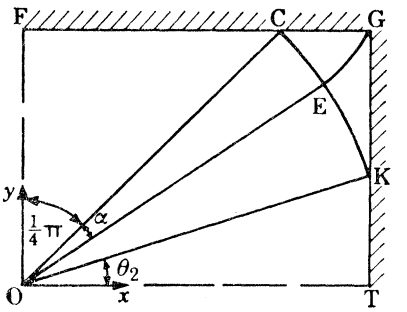

FIGURE 9. Regions for defining moment field when $1 < \xi \leqslant \sqrt{2}$.

The field (50) in OEK and the field (19) in OKT are together in equilibrium at O with the point load P_1 of equation (30) so that $f(\theta)$ must satisfy

$$\int_{\theta_2}^{\gamma} (1 - f(\theta))\, \mathrm{d}\theta + \tan\theta_2 = P_1, \tag{51}$$

where

$$\left.\begin{aligned} \gamma &= \tfrac{1}{4}\pi - \alpha, \\ \cos\theta_2 &= \xi/\sqrt{2}, \quad 0 \leqslant \theta_2 \leqslant \gamma. \end{aligned}\right\} \tag{52}$$

There remains the region EGK (figure 9) where we use orthogonal curvilinear coordinates u, v corresponding to a moment net with principal moments m_u, m_v as defined generally in § 3. We choose a net so that EG and EK are the characteristics $u = 0$ and $v = 0$ respectively and then define u, v by the conditions that the basic net angle ϕ of figure 2 satisfies

$$\left.\begin{aligned} \phi &= \gamma + v, \quad u = 0 \quad \text{on} \quad \text{EG}, \\ \phi &= \gamma - u, \quad v = 0 \quad \text{on} \quad \text{EK}. \end{aligned}\right\} \tag{53}$$

Thus u is the angular rotation of the tangent to EK (figure 9) between E and the end $v = 0$ of a characteristic $u =$ constant, and similarly for v with reference to the curve EG. The net will then be completely defined if we choose ϕ as a known function of (u, v) over the region. Here, we choose the simplest form satisfying (53), namely,

$$\phi = \gamma + v - u \tag{54}$$

over the region EGK. Geometrically, this net is simply a continuation of the Hencky–Prandtl net in CEG, with change of origin for u, and properties of the net can be obtained by replacing u by $u + \alpha$ in formulae given in § 4. We note that $h_1 > 0$, $h_2 > 0$ with the net existing over the whole region.

Next, we make the simple choice $m_u = 1$ (55)

throughout the region, whence using (54) and (55) in the equilibrium equation (7) we obtain

$$\frac{\partial m_v}{\partial u} = \frac{\partial m_v}{\partial v} + \frac{\partial}{\partial v}\left(\frac{h_1}{h_2}\frac{\partial m_v}{\partial v}\right) \tag{56}$$

as the governing equation for the remaining unknown m_v.

Continuity of moment and shear across the characteristic EG with the field (13) in CEG will be satisfied by (55) and

$$m_v = -1, \quad u = 0, \tag{57}$$

while the condition of zero edge moment on GK is, using (55),

$$m_v = -\tan^2\phi_e, \quad v = v_e(u), \tag{58}$$

where the edge values ϕ_e and v_e can be determined numerically as functions of u for given α from the properties of the net (54). It is easily shown analytically, that v_e decreases steadily as u increases in the range $0 \leqslant u \leqslant \gamma - \theta_2$ from G to K on the edge GK while the associated edge value ϕ_e decreases steadily from $\frac{1}{4}\pi$ at G to θ_2 at K.

On the third boundary EK, continuity of moment and shear with the field (50) will be satisfied, using (55), by

$$\partial m_v/\partial v = 0, \qquad v = 0, \tag{59}$$

$$m_v = f(\theta), \quad v = 0, \tag{60}$$

but this last equation is not a boundary condition restricting the present field in EGK. Instead equation (60) defines the previously unspecified $f(\theta)$ of (50) in terms of the solution for the present field, and if this field is statically admissible, then $|f(\theta)| \leqslant 1$ and the field (50) in OEK is also statically admissible.

We note that equation (51) is also not a restriction on the present field since P_1, given by (30), was found from a condition for overall equilibrium of the whole region OEGT; hence if we find statically admissible fields in the three subregions of figure 9 satisfying the equilibrium conditions at all boundaries, then (51) will automatically be satisfied by $f(\theta)$ from the field in EGK. Equation (51) is, however, useful as an overall check on the accuracy of numerical calculations for the field in EGK.

The differential equation (56) and the boundary conditions (57), (58), (59) give a determinate problem for m_v and by using the Crank–Nicholson form of finite differences to replace derivatives (see Smith 1965), the field in EGK was computed for cases 1 to 4 of table 1. The calculations were numerically stable and showed satisfactory convergence with decreasing mesh size down to a mesh size of interval $(\gamma - \theta_2)/100$ in u and $\alpha/50$ in v; for this finest mesh, the error in the overall check (51), expressed as a fraction of P_1, was less than 3×10^{-6} in all four cases. The results were satisfactory in giving $|m_v| \leqslant 1$ and hence this field completes a statically admissible field for the whole region OEGT (figure 9).

In the calculated field in EGK, the values of m_v increased monotonically with both u and v so that the extreme values were $m_v = -1$ on EG and $m_v = -\tan^2\theta_2$ at K. It was then found that these bounds for m_v, corresponding to a statically admissible field, could be deduced analytically direct from the governing equations (56) to (59). There are related initial discontinuities in $\partial^2 m_v/\partial v^2$ and $\partial m_v/\partial u$ at the corner G where $u = 0$, $v = \alpha$ but these discontinuities will not propagate into EGK for the parabolic equation (56) and for $u > 0$ we may assume that m_v and its derivatives are continuous functions of u and v. We consider the variation of m_v with v for given $u > 0$ and we shall use the term *smooth* for a maximum or minimum value to denote that it corresponds to $\partial m_v/\partial v = 0$.

For given u, varying v, the greatest algebraic value of m_v will be either (*a*) $m_v = M_e(u)$ (say) at the edge $v = v_e(u)$, or (*b*) $m_v = M(u)$ (say) at a smooth maximum at some point $v = v_1(u)$ in the range $0 \leqslant v_1 < v_e$, noting from (59) that this covers the case of the greatest value occurring at the end $v = 0$. Now M_e is given by the right-hand side of (58) in which, as noted earlier, ϕ_e decreases steadily as u increases, so that

$$\mathrm{d}M_e/\mathrm{d}u > 0. \tag{61}$$

On the other hand, $\partial m_v/\partial v = 0$, $\partial^2 m_v/\partial v^2 \leqslant 0$ at a smooth maximum, whence $\partial m_v/\partial u \leqslant 0$ from (56) since $h_1/h_2 > 0$, and then

$$\frac{\mathrm{d}M}{\mathrm{d}u} = \frac{\partial m_v}{\partial u} + \frac{\partial m_v}{\partial v}\frac{\mathrm{d}v_1}{\mathrm{d}u} = \frac{\partial m_v}{\partial u} \leqslant 0. \tag{62}$$

Thus $\mathrm{d}(M_e - M)/\mathrm{d}u > 0$ and in view of the initial condition (57) it follows that the greatest value of m_v for given positive u occurs at the edge $v = v_e$ where it is given by (58). Then, if any smooth maximum occurs for $0 \leqslant v < v_e$, there must also be a smooth minimum $m_v = m(u) < M(u)$ at some point between the smooth maximum and the even greater value at the edge. But for a minimum, $\partial m_v/\partial v = 0$, $\partial^2 m_v/\partial v^2 \geqslant 0$ whence by a similar argument to that for (62) above, we find

$$\mathrm{d}m/\mathrm{d}u \geqslant 0 \tag{63}$$

and then from (62), $\mathrm{d}(M - m)/\mathrm{d}u \leqslant 0$. Thus the amplitude $M - m$ cannot increase with u and it follows from (57) that a smooth maximum cannot occur for $u > 0$. Thus the value of m_v must increase monotonically with v for given u as found in the computations. Also, in view of (59), the end $v = 0$ will be a smooth minimum for which (63) indicates a value of m_v which increases monotonically with u. Thus for given u, the greatest value of m_v in EGK (figure 9) occurs on the edge GK where m_v increases monotonically from -1 at G to $-\tan^2\theta_2 \leqslant 0$ at K, while the least value occurs on EK where m_v increases monotonically between the same end values, so that $|m_v| \leqslant 1$ and the field is statically admissible.

7.3. $\sqrt{2} < \xi \leqslant \xi_1$

For this range of the aspect ratio ξ, the continuation of the circular arc CE (figure 5) divides OEGT into the two regions shown in figure 10. Then in the circular sector OEK we adopt the simple radial field (50), with $f(\theta)$ specified by continuity of moment across EK with the field in EKTG, so that the field (50) will be statically admissible in OEK if we can find a statically admissible field in EKTG.

In place of (51), the condition that the field (50) is in equilibrium with the point load P_1 at O is now

$$\int_0^\gamma (1 - f(\theta))\,\mathrm{d}\theta = P_1, \tag{64}$$

where $\gamma = \frac{1}{4}\pi - \alpha$ and P_1 is given by (30).

For the moment field in EKTG we again use (53) to define coordinates (u, v) in terms of the angular rotations of the tangents to the characteristics EK and EG. But the simple net (54) is no longer appropriate as we seek a net which satisfies also the symmetry condition that KT is a characteristic u = constant, which requires that

$$\phi = 0, \quad u = \gamma. \tag{65}$$

The conditions (53) and (65) are satisfied by any net of the form

$$\phi = \gamma - u + v - vF(u), \tag{66}$$

where
$$F(0) = 0, \quad F(\gamma) = 1, \tag{67}$$

and, for reasons given later, we also introduce the condition

whence
$$\left.\begin{aligned} F'(u) &\geqslant 0 \\ 0 \leqslant F(u) &\leqslant 1 \end{aligned}\right\} \quad (0 \leqslant u \leqslant \gamma). \tag{68}$$

The properties h_1, h_2 for a net of this type can be determined by assuming an expansion for h_2 as a power series in v with coefficients which are unknown functions of u. Then (4) and the given values of ρ_1 and ρ_2 on EK, EG respectively lead to recurrence relations for these functions of u,

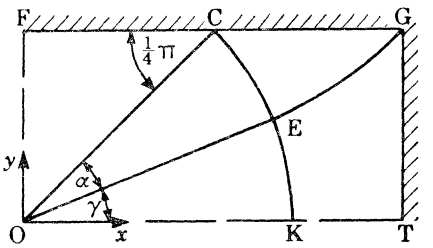

FIGURE 10. Regions for defining moment field when $\sqrt{2} < \xi \leqslant \xi_1$.

whence they can be evaluated numerically for a given $F(u)$. Then (5) enables coordinates (x, y) of points in the net to be evaluated, and the values of $v = v_e(u)$ on the edge GT can be obtained by interpolation. The method is straightforward and here we summarize only some relevant properties derived from the analysis. First, the conditions (68) are sufficient to ensure that

$$h_1 > 0, \quad h_2 > 0, \tag{69}$$

with the net existing over the whole region EKTG for which the relevant ranges of u, v, ϕ are

$$0 \leqslant u \leqslant \gamma; \quad 0 \leqslant v \leqslant v_e(u) \leqslant \alpha; \quad 0 \leqslant \phi \leqslant \phi_e(u) \leqslant \tfrac{1}{4}\pi. \tag{70}$$

Secondly, the values $v_e(u)$, $\phi_e(u)$ on the edge GT are both monotonic decreasing functions so that
$$\mathrm{d}v_e/\mathrm{d}u \leqslant 0, \quad \mathrm{d}\phi_e/\mathrm{d}u \leqslant 0, \tag{71}$$

while at the corner G, using the condition (75) below, we find

$$\left.\begin{aligned} \phi_e &= \tfrac{1}{4}\pi \\ v_e &= \alpha \end{aligned}\right\}, \quad \left.\begin{aligned} \mathrm{d}\phi_e/\mathrm{d}u &= -2 \\ \mathrm{d}v_e/\mathrm{d}u &= -1 \end{aligned}\right\} \quad (u = 0). \tag{72}$$

The choice of a suitable form for $F(u)$ is influenced by the related choice for m_u, and here we again adopt the simple form
$$m_u = 1 \tag{73}$$

through the region EKTG. Then (65) and (73) satisfy the conditions of zero twisting moment and zero shear force on the symmetry boundary KT.

The equation of equilibrium, as given by (7) with use of (4), (66) and (73), is

$$\frac{\partial}{\partial v}\left(\frac{h_1}{h_2}\frac{\partial m_v}{\partial v}\right) + (1 + vF'(u))\frac{\partial m_v}{\partial v} - 2F'(u)\,(1 - m_v) = (1 - F(u))\frac{\partial m_v}{\partial u}, \tag{74}$$

and the associated boundary conditions for m_v are (57), (58) and (59). Then (60) specifies $f(\theta)$ for the field (50) in the neighbouring sector OEK, while (64) serves as an overall check on numerical calculations for the present field in EKTG.

On $u = 0$, equation (74) with use of (57), (67) and (68) gives $\partial m_v/\partial u = -4F'(0) \leqslant 0$, whereas in view of (57) we require $\partial m_v/\partial u \geqslant 0$ on $u = 0$ to avoid violation of yield for small u. Hence we must introduce the further condition that

$$F'(0) = 0. \tag{75}$$

Equations (74), (57) (58) and (59) with a chosen $F(u)$ give a determinate problem for m_v, and a numerical solution was sought by finite differences. In the first instance, alternative calculations were carried out for the case $K = 5$ of table 1 with $F(u)$ equal to the square and then the cube of u/γ, which are the simplest forms satisfying the restrictions (67), (68) and (75) for $F(u)$. Both forms of $F(u)$ gave similar results with the fields satisfying the yield inequality except for very small values of u where m_v exhibited a minimum value < -1; though the violation of yield was very small, especially for the cubic form of $F(u)$. These results indicated, at least for the early part of the present range of ξ that the choice of $F(u)$ to give a statically admissible field depends particularly on the behaviour of the solution of the governing equations when u is small. To examine this behaviour, we introduce a dependent variable $T(u, v)$ defined by

$$T = 2 + (1 - F(u))^2 (m_v - 1), \tag{76}$$

and the equations (74), (57) to (59) for m_v then lead to the following equations for T:

$$(1 - F(u)) \frac{\partial T}{\partial u} = \frac{\partial}{\partial v}\left(\frac{h_1}{h_2}\frac{\partial T}{\partial v}\right) + (1 + vF'(u)) \frac{\partial T}{\partial v}, \tag{77}$$

$$T = 0, \quad u = 0, \tag{78}$$

$$\frac{\partial T}{\partial v} = 0, \quad v = 0, \tag{79}$$

$$T = 2 - (1 - F(u))^2 \sec^2 \phi_e, \quad v = v_e(u). \tag{80}$$

These equations are qualitatively similar to equations (56) to (59) for the field derived in the preceding range of ξ and, with appeal to certain of the conditions given in (68) to (71), the arguments of the preceding section can be repeated to obtain equations (61), (62) and (63) with M_e, M and m now applying to the solution for T. In particular, it follows that T is monotonic increasing in v for given u so that, using also (76), we have

$$\frac{\partial T}{\partial v} \geqslant 0, \quad \frac{\partial m_v}{\partial v} \geqslant 0, \tag{81}$$

for the present field. Thus the greatest value of m_v for given u occurs on the edge GT where it satisfies the yield inequality by virtue of (58) and (70), while the least value of m_v occurs on the boundary $v = 0$. Hence there will be no violation of yield if we can choose $F(u)$ so that $m_v \geqslant -1$ when $v = 0$, which requires from (76) that

$$T \geqslant 4F - 2F^2 \quad (v = 0). \tag{82}$$

We now seek an analytical expression for T for use in (82) by (a) introducing simplifications which tend to underestimate T and thus give a safe estimate for F, and (b) using simplifying approximations depending on u being small.

Equations (77) to (80) have a direct analogy as the governing equations for a problem of heat conduction along a rod, with T as temperature, u as time, v as distance along the rod, h_1/h_2 as

conductivity and $1-F(u)$ as specific heat per unit volume. The rod is initially at uniform temperature, and heat at a rate given by the $\partial T/\partial v$ term in (77) is supplied along the rod. The rod is insulated at the end $v=0$ while the section $v=v_e$, where v_e decreases with time, is maintained at a steadily increasing temperature in view of (80), (68) and (71). On physical grounds, we expect to underestimate the temperature at the end $v=0$, if (i) we omit the $\partial T/\partial v$ term in (77) since this corresponds to a positive heat supply in view of (68) and (81); (ii) we increase the specific heat by omitting the term $F(u)$ (non-negative by (68)) on the left-hand side of (77); and (iii) we underestimate the value of the conductivity h_1/h_2. Now for a net of the form (66) in EKTG, with $F(u)$ satisfying (68) and (75), it can be shown that the value of h_1/h_2 on $u=0$ increases monotonically with v from $h_1/h_2=1/(1+\alpha)$ at $v=0$ to $h_1/h_2=1$ at $v=\alpha$. On the other hand, h_1/h_2 tends to decrease with increasing u on $v=0$. We take $h_1/h_2=1/(1+\alpha)$ on the reasonable expectation for small u that the underestimate over most of the rod will outweigh the small overestimate near $v=0$ and give a net underestimate for T. With the above modifications, equation (77) becomes

$$\frac{\partial T}{\partial u}=\frac{1}{1+\alpha}\frac{\partial^2 T}{\partial v^2}. \tag{83}$$

We shall also underestimate T for $u>0$ if we neglect the decrease in the effective length v_e of the rod by taking this length as constant at its initial value $v_e=\alpha$; also for small u we approximate to (80) by using (67), (72) and (75) to retain only the first-order term, whence (80) becomes

$$T=8u, \quad v=\alpha. \tag{84}$$

Equations (83), (78), (79) and (84) correspond to a standard problem of heat conduction which is easily solved, for example by Laplace transforms (Carslaw & Jaeger 1959), and for small values of u, the dominant term in an asymptotic expansion of the solution for T gives

$$\left.\begin{aligned} T&=\frac{4\alpha^2(1+\alpha)\exp(-\zeta^2)}{\zeta^5\sqrt{\pi}} \quad (v=0),\\ \text{where}\quad \zeta&=\tfrac{1}{2}\alpha\left(\frac{1+\alpha}{u}\right)^{\frac{1}{2}}. \end{aligned}\right\} \tag{85}$$

Hence if we choose

$$F(u)=\frac{C\alpha^2(1+\alpha)\exp(-\zeta^2)}{\zeta^5\sqrt{\pi}}, \tag{86}$$

the condition (82) will be safely satisfied if $C\leqslant 1$. The value of C is not open to choice, but is determined by the condition $F(\gamma)=1$ in (67) which gives

$$\left.\begin{aligned} C&=\frac{\sqrt{(\pi)}\,\zeta_1^3\exp(\zeta_1^2)}{4\gamma},\\ \text{where}\quad \zeta_1&=\tfrac{1}{2}\alpha\left(\frac{1+\alpha}{\gamma}\right)^{\frac{1}{2}} \end{aligned}\right\} \tag{87}$$

and computations of (87) for the present range of ξ show that the largest value of C in this range is $C=0.24\ldots$, occurring for the changeover case $\xi=\xi_1$. Thus (86) satisfies the inequality (82) by a factor of at least four, which should amply cover approximations made for small u; hence (86) should lead to a statically admissible field for small values of u.

For the cases 5 to 11 of table 1, with the use of (86) in the net (66), the solution of (74), (57) to (59) for m_v was obtained numerically using finite differences with the Crank–Nicholson representation of derivatives. The calculations were numerically stable and showed satisfactory convergence with decreasing size of mesh, down to a mesh of intervals $\gamma/200$ in u and $\alpha/100$ in v; for this

finest mesh, the error in the overall check (64) was in all cases less than 3×10^{-5} expressed as a fraction of P_1.

The fields were statically admissible in all cases 5 to 11 of table 1 and verified in particular the prediction of equation (81) that m_v increases monotonically with v for given u. Thus the greatest value of m_v for given u occurs on the edge GT where it satisfies the yield inequality by virtue of the boundary condition. The least value of m_v for given u occurs on the boundary EK where

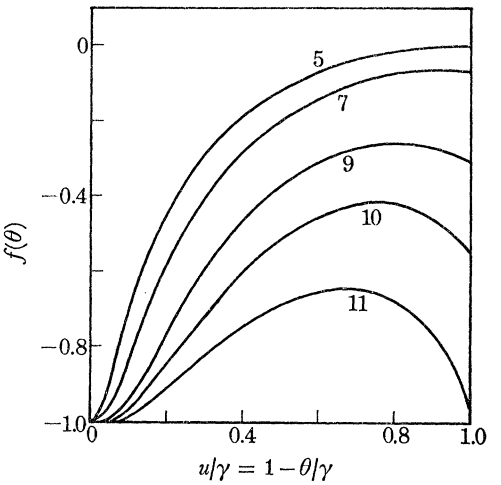

FIGURE 11. Variation of $m_r = f(\theta)$ on EK in figure 10 for cases 5, 7, 9 to 11 of table 1.

TABLE 1. COLLAPSE LOAD FOR MECHANISM AND MOMENT FIELD OF FIGURE 5

case no.	$\frac{\alpha}{\text{rad}}$	aspect ratio, $\xi = a/b$	collapse load P
—	0	1	8
1	0.03927	1.0801	8.0235
2	0.07854	1.1636	8.0895
3	0.11781	1.2506	8.1928
4	0.15708	1.3416	8.3290
5	0.19635	1.4367	8.4945
6	0.23562	1.5363	8.6867
7	0.27489	1.6408	8.9032
8	0.31416	1.7505	9.1420
9	0.35343	1.8657	9.4015
10	0.39270	1.9870	9.6804
11	0.43197	2.1147	9.9775
12	0.47019	2.2456	$4+2\pi$

$v = 0$ and $m_v = f(\theta)$ of the field (50), and the variation of $f(\theta)$ with $u = \gamma - \theta$ on EK is shown for selected cases in figure 11. For the later cases, as u increases, $f(\theta)$ increases to a maximum and then decreases, and for case 11 the yield condition $m_v \geqslant -1$ is only satisfied by a small margin at the end $u = \gamma$. This behaviour is to be expected; thus our choice of $F(u)$ ensures that $f(\theta)$ increases initially with u, whereas the equilibrium condition (64) controls the average value of $f(\theta)$, namely $1 - P_1/\gamma$, which decreases steadily as ξ increases in the present range, and for case 12 where $\xi = \xi_1$ and $P_1 = 2\gamma$ from (32), (34) and (52), the average value of $f(\theta)$ is the yield value $m_v = -1$.

Figure 11 indicates that the preceding assumptions will only lead to a statically admissible field for values of ξ up to a value slightly greater than that for case 11 in table 1. For the remaining

part of the range up to $\xi = \xi_1$ for case 12, we control the value of $f(\theta)$ by introducing an extra boundary condition for m_v, namely

$$m_v = f(\theta) = -1 + F_1(u) \quad (v = 0, \quad \theta = \gamma - u), \tag{88}$$

where

$$F_1(0) = 0, \tag{89}$$

and $F_1(u)$ is to be a chosen monotonic increasing function of u, with its overall magnitude determined by (64); these conditions ensure that $f(\theta) \geqslant -1$, and we note that $F_1(u) \equiv 0$ for the change-over case 12.

We must now modify either the assumed moment net or the form of m_u in order to introduce some function of u which can act as an extra parameter for given u so that the additional boundary condition (88) can be satisfied. For computation it is simpler to insert the extra parameter in the form of m_u, so we retain the previous net (66), with $F(u)$ given by (86), and replace $m_u = 1$ by the form

$$m_u = 1 - G(v)\, F_2(u), \tag{90}$$

where

$$F_2(0) = F_2'(0) = 0, \tag{91}$$

$$G(0) = 0, \quad G(v) > 0 \quad \text{for} \quad v > 0, \tag{92}$$

and $G(v)$ is to be a chosen function of v, while $F_2''(u)$ provides the necessary extra parameter to be found in the computations for the field m_v.

The conditions (89), (91) and (92) with m_u given by (90) are such that all the continuity conditions of moment and shear force on the boundaries EK, EG (figure 10) will be satisfied if m_v satisfies (88) and the previous boundary conditions (57) and (59), while the edge condition (58) is now modified to

$$m_v = -(1 - G(v_e)\, F_2(u)) \tan^2 \phi_e, \quad v = v_e(u), \tag{93}$$

and the equation (7) of equilibrium becomes

$$\frac{\partial}{\partial v}\left(\frac{h_1}{h_2}\frac{\partial m_v}{\partial v}\right) + (1 + vF'(u))\frac{\partial m_v}{\partial v} - 2F'(u)\,(1 - m_v) - (1 - F(u))\frac{\partial m_v}{\partial u}$$
$$= G(v)\left[\frac{\partial}{\partial u}\left(\frac{h_2}{h_1}F_2'(u)\right) + (1 - F(u))\,F_2'(u) - 2F'(u)\,F_2(u)\right] - (1 + vF'(u))\,F_2(u)\,G'(v). \tag{94}$$

For chosen $F_1(u)$ and $G(v)$, equation (94) with boundary conditions (57), (59), (88) and (93) for m_v and initial conditions (91) for $F_2(u)$ gives a determinate problem for m_v and F_2 which can be solved numerically by using finite differences and marching out from $u = 0$.

There is, however, the further boundary condition that the shear force q_u is zero on the symmetry line KT (figure 10), which from (90) and (8) requires that

$$F_2'(\gamma) = 0, \tag{95}$$

though this is not in fact an *independent* boundary condition. Thus the solution of the preceding equations will give a moment field in EKTG (figure 10) which, together with the field (50) in the sector OEK, will satisfy (*a*) equilibrium with zero distributed load over the whole leaf OEGT and with the point load P_1 at O, and (*b*) the correct boundary conditions round OEGT except possibly on KT. But we stipulated that $F_1(u)$ in (88) is chosen to satisfy (64) in which the point load P_1 was found by considering the overall equilibrium of OEGT for moments about GT on the assumption of no contribution to this equilibrium from shear forces on KT. It follows that if the present field could be computed exactly from (94) and the associated boundary conditions,

then any shears q_u found on KT must contribute no resultant couple about the edge GT. But, since $q_u = \partial m_u/h_1 \partial u$ on the straight boundary KT, this condition of zero resultant couple is

$$F_2'(\gamma) \int_0^{v_e(\gamma)} \frac{G(v)\,(a-x)\,h_2}{h_1} \mathrm{d}v = 0 \quad (u = \gamma), \tag{96}$$

in which, from (92) the integral is positive, so that (96) implies that (95) would automatically be satisfied by an exact solution of (94) and its associated boundary conditions (57), (59), (88), (91) and (93).

Hence (95) is not a condition which has to be taken into account, *a priori*, in computations of the field; instead, the smallness of the computed left-hand side of (96), expressed as a fraction of the corresponding moment $P_1 a$ of the point load about the edge, furnishes a useful overall check on the accuracy of the calculation.

We turn now to the choice of $F_1(u)$ and $G(v)$, and here trial computations, using simple power forms for F_1 and G gave statically admissible fields except for small values of u, where the yield conditions $m_u \leqslant 1$ and $m_v \geqslant -1$ were violated, though only by small fractions. Accordingly, an approximate analysis of the behaviour of the solution for small u was carried out, retaining only the dominant term of any one type in the equations, and replacing h_1/h_2, which varies between $1/(1+\alpha)$ and 1 on $u = 0$, by a constant k assumed to lie in the range $1/(1+\alpha) \leqslant k \leqslant 1$. The resulting equations of the thermal conduction type were then analysed by using the Laplace transformation with respect to u. The result of this rather lengthy analysis indicated that for any choice of k in the relevant range $1/(1+\alpha) \leqslant k \leqslant 1$, there would be no violation of yield for small u if we choose, in particular,

$$\left.\begin{aligned} F_1(u) &= C_1 F(u), \\ G(v) &= \exp(-\alpha/4v), \end{aligned}\right\} \tag{97}$$

where C_1 is determined by (64) and varies between 0.812 and zero for the present range of ξ from case 11 to case 12 of table 1.

By using (97) and finite differences with the Crank–Nicholson representation of derivatives, the exact equations (94), (57), (59), (88), (91) and (93) were solved numerically for cases 11 and 12 of table 1. The computations were numerically stable and showed satisfactory convergence with decreasing size of mesh, down to a mesh of intervals $\gamma/200$ in u and $\alpha/100$ in v. For this finest mesh, the error in the overall check (96), expressed as a fraction of $P_1 a$ was less than 6×10^{-5} in both cases 11 and 12. Statically admissible fields were obtained in EGTK (figure 10) in each case with the following features. The values of m_u decrease monotonically with increasing u and v between extreme values $m_u = 1$ on EG and EK and $m_u = 0.835, 0.925$ at T for cases 11 and 12 respectively. For case 11, m_v increases monotonically with v for given u except near $u = \gamma$ where m_v develops a maximum moving into the region from the edge and increasing slowly in magnitude as u increases; the extreme values of m_v are -1 on EG and 0.00215 on KT near T. For case 12, m_v increases monotonically with v for given u over the whole region with extreme values of $m_v = -1$ on EG and EK, and $m_v = 0$ at T.

Finally we note that since $m_v = f(\theta) = -1$ on EK (figure 10) for case 12, the field (50) used in OEK is the same as the field (18) used in OCE, and together with the field (17) in OFC they satisfy the normality rule in relation to the mechanism of figure 8 as well as the mechanism defined in terms of figure 5; while the field found in EGTK for case 12 is statically admissible for the undeflected outer portion of the plate in figure 8. Thus the field obtained for case 12 combines with either of the two alternative mechanisms when $\xi = \xi_1$ to give an exact solution.

8. A Statically admissible moment field when $\xi > \xi_1$

For $\xi > \xi_1$ the mechanism is the pyramid cum cone illustrated in plan in figure 8, and for the associated moment field we need again consider only the first quadrant in view of symmetry. This quadrant can be divided into two rectangular regions as illustrated in figure 12 where in OFLM we use the statically admissible field previously found for $\xi = \xi_1$, corresponding to the change of mechanism.

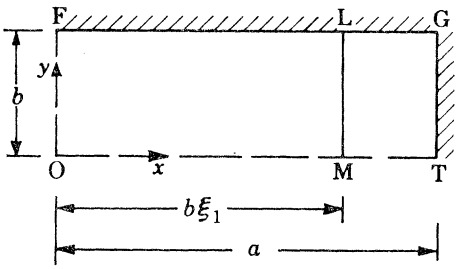

Figure 12. Regions for defining moment field when $\xi > \xi_1$.

It remains to find a statically admissible field in LGTM, for which we use rectangular coordinates x, y as in figure 12. This field must then satisfy first, the equation of equilibrium for zero load, namely

$$\frac{\partial^2 m_x}{\partial x^2} + 2\frac{\partial^2 m_{xy}}{\partial x\,\partial y} + \frac{\partial^2 m_y}{\partial y^2} = 0, \tag{98}$$

secondly, the boundary conditions

$$\left.\begin{aligned} m_x &= 0, && x = a,\\ m_y &= 0, && y = b,\\ m_{xy} &= 0, \quad q_y = 0, && y = 0, \end{aligned}\right\} \tag{99}$$

and thirdly, continuity conditions with the field of case 12 on LM. It is very probable that a statically admissible field could be found in LGTM such that all component moments and shears were continuous across LM with the field of case 12; but this would probably require extensive numerical calculations for a series of aspect ratios $\xi > \xi_1$. This can be avoided if we make use of the fact that the rules of limit analysis permit LM to be a line of discontinuity subject only to the Kirchoff conditions of continuous normal moment and shear reaction.

For case 12, LM is a simply supported edge with zero normal moment

$$m_x = 0, \quad x = \xi_1 b, \tag{100}$$

while the edge shear reaction $V(y)$ defined by

$$\frac{\partial m_x}{\partial x} + 2\frac{\partial m_{xy}}{\partial y} = V(y), \quad x = \xi_1 b, \tag{101}$$

was evaluated numerically in the computations for the field of case 12. Here we need note only the results that $V(y)$ is of negative sign, corresponding to an upward supporting reaction, along the whole edge and that the total reaction upwards on the plate edge LM in case 12 is (rounded value)

$$-\int_0^b V(y)\,dy = 0.69. \tag{102}$$

Then for $\xi > \xi_1$ the essential conditions to be satisfied on LM by the field in LGTM (figure 12) are equations (100) and (101) where $V(y)$ is known from the case 12 field.

It is easily verified that the simple field

$$\left.\begin{aligned} m_x = 0, \quad m_y = 0, \quad m_{xy} = \frac{1}{2}\int_0^y V(y)\,\mathrm{d}y, \\ q_x = \tfrac{1}{2}V(y), \quad q_y = 0, \end{aligned}\right\} \tag{103}$$

in LGTM satisfies the equilibrium equation (98) and the boundary conditions (99), (100) and (101). For this field, the principal moments are

$$m_1 = -m_2 = |m_{xy}| \tag{104}$$

and since $V(y)$ is of constant negative sign, it follows from (102) and (103) that the maximum principal moments occur for $y = b$ and are numerically equal to 0.345. Hence the yield condition is well satisfied over the whole region LGTM and the field (103) is statically admissible for all $\xi > \xi_1$.

9. Off-centre point load

To derive and justify exact solutions for all possible cases of off-centre load on a simply supported rectangular plate would involve a major independent investigation beyond the scope of the present paper. Here we note only some special cases of off-centre load for which the exact solution can be simply derived from the preceding solution for a central point load.

With reference to figure 13*a*, a point load acts at I on the simply supported plate PQRS and we consider the case where each of the rectangular regions 1 to 4 has an aspect ratio (longer side/shorter side) $\leqslant 2.1147 = \xi_2$ (say) corresponding to case 11 of table 1. The exact solution for this off-centre load is obtained by regarding each region in turn as one quadrant of a simply-supported rectangular plate subjected to a point-load at its centre I. Then we use in each region the central-load solution corresponding to figure 5, with OF, OT in figure 5 identified with the shorter and longer sides of a region in figure 13*a*. We specify that the mechanisms in the four regions have a common vertex I′ corresponding to O′ in figure 5. The conditions on the junctions HI, JI, KI and LI in figure 13*a* will then correspond variously to the conditions on OF and OT in figure 5. But for aspect ratio $\leqslant \xi_2$, the moment-field found for the central load satisfies the conditions of unit normal moment, zero twisting moment and zero shear along both OF and OT; also, the mechanism of figure 5 for a central load involves a plane leaf through O′ and the corresponding edge for both OF and OT. It follows that the central-load solutions in the four regions of figure 13*a* will fit together to give a combined moment field and mechanism satisfying all the conditions of an exact solution for the off-centre load at I on the plate PQRS.

We note that when OT/OF $> \sqrt{2}$ in the field of figure 5, the moment m_r is zero along OF but not along OT; hence the preceding solution for the off-centre load may involve discontinuities in the tangential moment along a junction such as IL in figure 13*a* which corresponds to OT of figure 5 for region 1 and to OF for region 2. This type of discontinuity is permissible in a statically admissible field; it is not necessarily an essential feature of the problem of the off-centre load, since the discontinuity occurs in a rigid leaf where the moment field is not determinate. It is very probable that an alternative statically admissible field exists with no discontinuities in component moments.

The exact collapse load for the off-centre load at I (figure 13*a*) will be the mean of the exact central collapse loads (table 1 and figure 7) for rectangles of aspect ratios corresponding to those

of the rectangular regions 1 to 4, subject to the condition that all those aspect ratios are $\leqslant \xi_2$. For region 1, this requires that I lies on or between lines making angles arctan $(1/\xi_2)$ with the edges PS and PQ respectively, with similar conditions for regions 2 to 4 in terms of lines from the corners Q, R and S. For $1 \leqslant \xi < 0.5\,(\xi_2 + 1/\xi_2) = 1.345$, this leads to the condition that the preceding solution is exact if the off-centre load acts at any point in a central region of octagonal

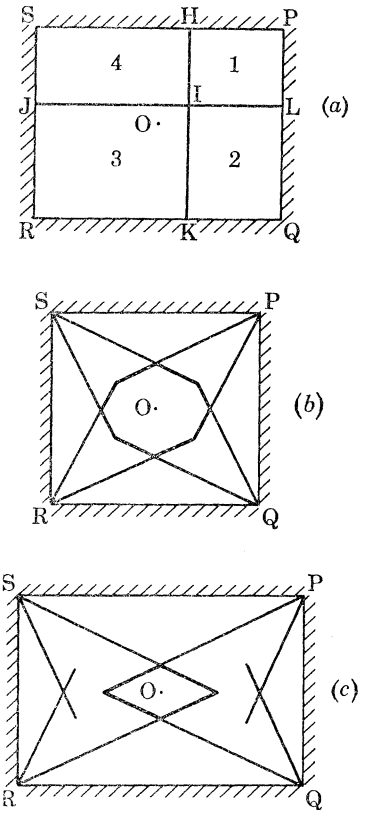

FIGURE 13*a* to *c*. Off-centre load in central region of plate.

shape as illustrated in figure 13*b*; while for $0.5\,(\xi_2 + 1/\xi_2) \leqslant \xi < \xi_2$, the relevant central region is of the rhombus shape illustrated in figure 13*c*.

When $\xi = \xi_2$ the rhombus of figure 13*c* shrinks to the central point O and for $\xi > \xi_2$ there is no central region such that all four regions of figure 13*a* have aspect ratios $\leqslant \xi_2$. However, for $\xi > \xi_2$, central-load solutions can be combined to give an exact solution in the special case where a point load acts on the longer centre-line at any point whose distance from the nearer short edge is $\geqslant b/\xi_2$.

With reference to figure 14, PQRS is a rectangular plate of centre O and aspect ratio $> \xi_2$, with a point load acting at I on the longer centre-line Ox at a distance $L \geqslant b/\xi_2$ from the nearer short edge PQ. We consider the solution in terms of the two rectangular regions 1, 2 with junction on HIK. For region 1, we use the central-load solution given by regarding this region as one half of a rectangular plate with centre I and aspect ratio $(2a - L)/b > \xi_2$, subjected to a point load at I. For all such aspect ratios, the conditions given by the central-load solution on HI and IK are those previously stated on OF in figure 5, noting that the same conditions hold on the shorter centre-line of figure 8 which gives the relevant central-load solution when $(2a - L)/b > \xi_1$. Similarly, for region 2 of figure 14, we use the central load solution given by regarding this

region as one half of a rectangular plate with centre I and aspect ratio equal to the larger of L/b and b/L, and we specify that the mechanism has the same vertex as the mechanism for region 1. The conditions on HI and IK for region 2 correspond to those on OF (figure 5) for $L \geqslant b$ and to those on OT for $b/\xi_2 \leqslant L < b$. In either case, the central-load solutions for the two regions fit on HIK to give an exact solution for the load at I on the plate PQRS of figure 14.

Thus if $\xi > \xi_2$ and the point load acts on the longer centre-line at any point whose distance L from the nearer short edge is $\geqslant b/\xi_2$, the exact collapse load is the mean of the central collapse loads (table 1 and figure 7) for rectangles of aspect ratios $(2a-L)/b$ and the larger of L/b and b/L. In particular if $a > L \geqslant b\xi_1$, both the relevant collapse loads and hence their mean are equal to $4+2\pi$ corresponding to the plate behaving effectively as an infinitely long strip.

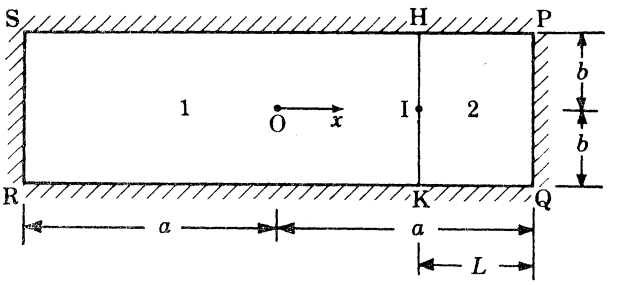

FIGURE 14. Off-centre load on longer centre-line.

For $\xi \leqslant \xi_2$, the above solution for a load on the longer centre-line is simply a special case of a load acting in the central region of figure 13*b* or 13*c*.

The use of ξ_2 in defining the scope of the above solutions for an off-centre load is not intended to imply that the value ξ_2 is of *intrinsic* significance in the present problem. Instead, the use of ξ_2 arises from the particular method of obtaining a statically admissible field over the rigid region OEGT of figure 5 for the central load problem. Thus for cases 1 to 11 of table 1 we found a field such that $m_u = 1$ in OEGT. But to cover the range of cases 11 and 12 the choice $m_u = 1$ was abandoned for the portion EGTK (figure 10), solely because of the much greater computational difficulties in the alternative procedure of retaining $m_u = 1$ and finding a suitable moment net numerically over a fine mesh. It is very probable that a statically admissible field with $m_u = 1$ in OEGT (figure 5) exists also for the range of cases 11 and 12 to give in particular, $m_u = 1$ with zero shear and twisting moment along OT. If so, the scope of the preceding solutions for an off-centre load can be extended by replacing ξ_2 in the arguments by the larger value $\xi_1 = 2.2456$ corresponding to case 12 of table 1.

10. Conclusions

The solution obtained for the simply supported rectangular plate under a central point load leads to two main conclusions. First, it indicates that an apparently simple problem of limit analysis can require a relatively complex exact solution; such complexity, rather than the non-existence of exact solutions, is the probable reason why so few exact solutions have been found in this field for other than a symmetrically loaded circular plate. Secondly, the simple upper bounds of yield-line theory give estimates of the collapse load (figure 7) for varying aspect ratio which are in error by a maximum of less than 4 %. This error is certainly within the accuracy with which limit analysis can be regarded as representing actual conditions in reinforced concrete slabs.

11. Addendum

After the present paper had been submitted for publication, the author learnt of a recent paper by Collins (1971) which, *inter alia*, anticipated certain salient features of the present solution for the problem of the central load on a simply supported rectangular plate. In this paper, Collins extended a useful and elegant analogy, originated by Johnson (1969), between problems in plane strain and in plate bending for rigid perfectly plastic material. As one example, he derived the exact mechanism (present figure 5) and the exact collapse load (QR, present figure 7) for the central load case, though these results were only presented as an upper bound solution, since a statically admissible moment field in the rigid leaf OEGT (present figure 5) had not been found. Collins also showed that the yield-line solution corresponding to the present figure 8 is exact for aspect ratios $a/b \geqslant 3.10$, i.e. for the later part of the full range $a/b \geqslant 2.25$ for which this solution has here been shown to be exact.

References

Carslaw, H. S. & Jaeger, J. C. 1959 *Conduction of heat in solids*. Oxford: Clarendon Press.

Collins, I. F. 1971 On an analogy between plane strain and plate bending solutions in rigid/perfect plasticity theory. *Int. J. Solids Struct.* **7**, 1057–1073.

Fox, E. N. 1968 The existence of exact solutions in Limit Analysis for homogeneous isotropic plates of rigid perfectly-plastic material. *Engineering plasticity* (ed. J. Heyman and F. A. Leckie), pp. 147–181. Cambridge University Press.

Johansen, K. W. 1942 *Brudlinieteirier*. Copenhagen: I kommission hos Teknisk Forlag. (English translation, *Yield-line theory*. London: Cement and Concrete Association, 1962.)

Johnson, W. 1969 Upper bounds to the load for the transverse bending of flat rigid-perfectly plastic plates. *Int. J. Mech. Sci.* **11**, 913–938.

Mansfield, E. H. 1957 Studies in collapse analysis of rigid-plastic plates with a square yield diagram. *Proc. R. Soc. Lond.* A **241**, 311–338.

Prager, W. & Hodge, P. G. Jnr 1951 *Theory of perfectly plastic solids*. New York: Wiley.

Sawczuk, A. & Hodge, P. G. Jnr 1968 Limit analysis and yield-line theory. *J. Appl. Mech.* **35**, 357–362.

Smith, G. D. 1965 *Numerical solution of partial differential equations*. Oxford: Clarendon Press.

Wood, R. H. 1965 New techniques in nodal-force theory for slabs. M.C.R. special publication: *Recent developments in yield-line theory*, pp. 31–62. London: Cement and Concrete Association.

Wood, R. H. 1968 Some controversial and curious developments in the plastic theory of structures. *Engineering plasticity* (ed. J. Heyman and F. A. Leckie), pp. 665–691. Cambridge University Press.

PHILOSOPHICAL TRANSACTIONS OF THE ROYAL SOCIETY A MATHEMATICAL, PHYSICAL & ENGINEERING SCIENCES